Programmable Metasurface for Simultaneously Wireless Information and Power Transfer System

CHANG Mingyang[1], HAN Jiaqi[1], MA Xiangjin[1], XUE Hao[1], WU Xiaonan[1], LI Long[1], CUI Tiejun[2]

(1. Key Laboratory of High-Speed Circuit Design and EMC of Ministry of Education, School of Electronic Engineering, Xidian University, Xi'an 710071, China;
2. State Key Laboratory of Millimeter Waves, Southeast University, Nanjing 210096, China)

DOI: 10.12142/ZTECOM.202202008

https://kns.cnki.net/kcms/detail/34.1294.TN.2020506.1130.002.html, published online May 6, 2022

Manuscript received: 2022-04-18

Abstract: Implementing self-sustainable wireless communication systems is urgent and challenging for 5G and 6G technologies. In this paper, we elaborate on a system solution using the programmable metasurface (PMS) for simultaneous wireless information and power transfers (SWIPT), offering an optimized wireless energy management network. Both transmitting and receiving sides of the proposed solution are presented in detail. On the transmitting side, employing the wireless power transfer (WPT) technique, we present versatile power conveying strategies for near-field or far-field targets, single or multiple targets, and equal or unequal power targets. On the receiving side, utilizing the wireless energy harvesting (WEH) technique, we report our work on multi-functional rectifying metasurfaces that collect the wirelessly transmitted energy and the ambient energy. More importantly, a numerical model based on the plane-wave angular spectrum method is investigated to accurately calculate the radiation fields of PMS in the Fresnel and Fraunhofer regions. With this model, the efficiencies of WPT between the transmitter and the receiver are analyzed. Finally, future research directions are discussed, and integrated PMS for wireless information and wireless power is outlined.

Keywords: programmable metasurface; simultaneously wireless information and power transfers; wireless energy harvesting; wireless power transfer

Citation (IEEE Format): M. Y. Chang, J. Q. Han, X. J. Ma, et al., "Programmable metasurface for simultaneously wireless information and power transfer system," *ZTE Communications*, vol. 20, no. 2, pp. 48 – 62, Jun. 2022. doi: 10.12142/ZTECOM.202202008.

1 Introduction

The wireless communication technology has developed rapidly in the past two decades and has become an indispensable part of our daily lives. Especially with the Internet of Things (IoT) concept, the combination of people, data, and things through networks makes network connections more relevant and valuable. People can interact with various devices more conveniently, which significantly facilitates our production and life and penetrate many fields such as home automation, industrial automation, and medical assistance. With the needs of society and the development of science and technology, 5G technologies have gradually entered our lives[1]. Compared with the previous generations of mobile communications, it has a better user experience rate, connection density, peak rate, and other characteristics, which can meet the mobile data growth demands of over a thousand times in the future[2]. This provides the possibility for the further development of IoT. The future wireless environment will rely on large-scale communications and IoT to meet the increasingly intelligent world, which requires us to deploy millions of low-power sensor networks, actuators, and small computing devices in the environment[3]. For the sustainable development of the entire wireless sensor network, how to adaptively provide enough energy for a large number of sensors has become a challenging problem we must face now.

To meet the intensive energy requirements for 5G and 6G communications, the concept of simultaneous wireless information and power transfers (SWIPT) was proposed and discussed comprehensively by the communication commu-

This work was supported by the National Key Research and Development Program of China under Grant Nos. 2017YFA0700201, 2017YFA0700202, 2017YFA0700203, and 2021YFA1401001, the 111 Project under Grant No.111-2-05, National Natural Science Foundation of China under Grant No. 62001342, Key Research and Development Program of Shaanxi under Grant No. 2021TD-07, and Outstanding Youth Science Foundation of Shaanxi Province under Grant No.2019JC-15.
LI Long and Cui Tiejun are the corresponding authors.

nity[4–12]. Considering the wireless power conveying and wireless power collection for modern wireless communication networks is the notable characteristic of SWIPT. Thus, theoretical analyses and model constructions on wireless power transfer (WPT) efficiency are the main topics for system level researchers[13–18]. The fundamentals of SWIPT for a realizable future communication network are established based on linear and nonlinear models, which point out a clear path for the hardware level designers.

The core techniques to implement SWIPT are WPT and wireless energy harvesting (WEH). The WPT technology was firstly proposed by Nikola TESLA. Because of its potential application value, it was selected by the *Technology Review* magazine as one of the ten scientific research directions that would bring considerable changes to human production and lifestyle in the future. In recent two decades, great efforts have been made on the inductive or capacitive coupling[19–22], achieving a satisfying transmission efficiency of over 70% under several watts[23]. However, this technique can be classified as a nonradiative type, which operates at kilohertz or megahertz within inductive near-field or Fresnel near-field. Therefore, it is not feasible to apply this resonance method to build a SWIPT network due to the transmission range and the working frequency limitations. Alternatively, the radio frequency (RF) waves can be emitted into free space through antennas, which is coined as the radiative-type WPT[24–27]. By manipulating the radiated waves, one could direct the wireless energy to targets efficiently[28]. It is worth noting that when adopting the radiative-type WPT, unlike the nonradiative-type WPT, a receiving device should be applied to harvest energy and convert RF power into direct circuit (DC) power, which is enabled by the WEH technique[29–31]. The receiving device, which is called the rectenna or rectifying antenna, consists of a conventional receiving antenna and a rectifying circuit. Nevertheless, the rectifying efficiency of the rectenna severely depends on the input power level. Besides, the performance of the receiving antenna also limits the captured wireless power for the rectifying circuit. From the above research, it can be clearly observed that the existing WPT and WEH techniques mainly employ the typical RF and microwave technologies. As a result, both the WPT and WEH developments need a revolutionary methodology.

Metamaterials and metasurfaces were proposed in the early 21st century, providing a new way to observe the physical world[32]. Previous studies on this topic focused on the basic theory and anomalous phenomenon[33–35]. Researchers in the WPT and WEH communities keenly adopted these advanced materials to enhance the power transmission efficiency and design novel devices[36–46]. However, such analog metamaterials possess an intrinsic issue that has fixed functionality after fabrication. In 2014, CUI et al. proposed the programmable metasurface (PMS), introducing digital coding for designing versatile metamaterials[47]. Using active components on each meta-atom, one can regulate the metasurface through an external field-programmable gate array (FPGA), which greatly enriches the original analog metamaterials. Recently, we reported an adaptively smart WPT based on a 2-bit PMS, which could continuously transmit the wireless power to the receiver even though the target was moving[48]. In addition to transmitting wireless power, wireless information can be envisioned when the space-time-coding (STC) technique is applied to PMS[49–54]. The STC technique introduces period time modulations to each programmable meta-atom which allows us to modulate digital signals directly without using the traditional communication system architecture[55–58]. More exciting studies on microwave imaging and recognition were also reported to examine the information PMS[59–64]. The wireless communication community further extends this methodology to improve the communication channels. Under this application scenario, the information PMS was coined as a reconfigurable intelligent surface (RIS)[65–67].

So far, we have briefly reviewed the concepts and relationships of SWIPT, WPT, WEH, information PMS, and RIS. However, it can be clearly seen that a system-level solution to SWIPT based on PMS is still unavailable. In this paper, we develop a feasible strategy for SWIPT to integrate wireless information and wireless power using PMS. The rest of this paper is organized as follows. We first overview the PMS-based SWIPT for the future smart cities in Section 2. Then the adaptively smart WPT strategy using PMS in Section 3 is discussed. After that, Section 4 presents the WEH metasurfaces and transmission efficiency analyses for the PMS-based SWIPT. Finally, in Section 5, we direct the future research and conclude this paper.

2 Overview of PMS-Based SWIPT for Smart City

With the advent of the 5G and 6G era, the IoT technology will inevitably usher in new development. People's production and lives will become more intelligent. More and more sensor networks will inevitably become an essential part of our interaction with the outside world. Traditional battery power supply requires manual replacement of the battery periodically to ensure the normal operation of the sensor network, which takes time and effort and causes serious pollution to the environment. The WPT technique is undoubtedly a good solution. To improve its transmission efficiency, this paper proposes a SWIPT system based on PMS. A typical SWIPT system has three forms[6].

• SWIPT. It can transmit wireless power while transmitting traditional wireless information signals. After the wireless device receives the power, the wireless energy can be stored in the battery of the wireless device after a series of conversions, which can be used to supply power to the corresponding electrical equipment, as shown in Figs. 1(a) and 1(b).

• Wirelessly powered communication networks (WPCNs).

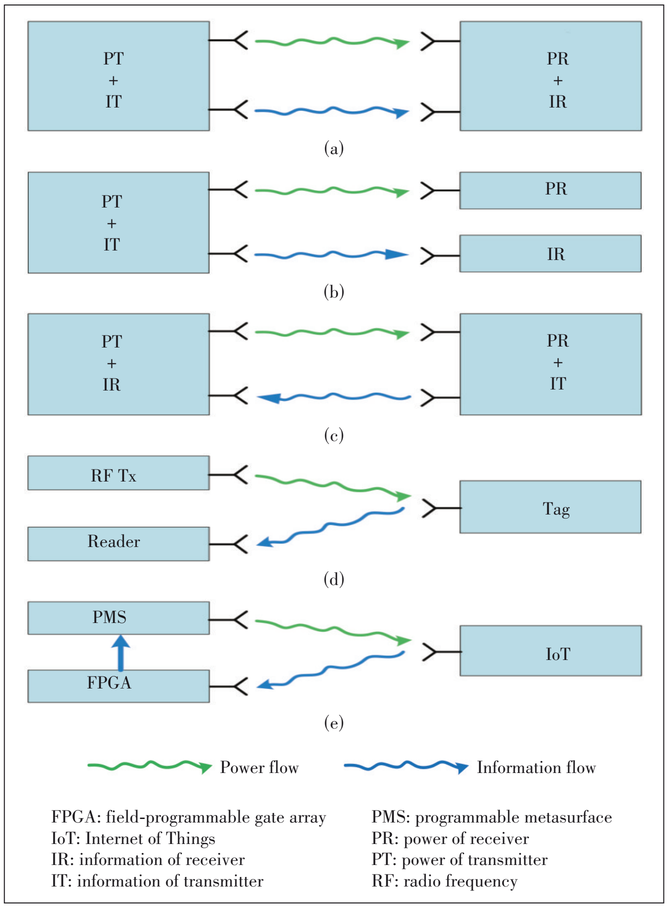

▲**Figure 1. Different forms of wireless information and power transfers (WIPT): (a) SWIPT with co-located receivers; (b) SWIPT with separated receivers; (c) wirelessly powered communication networks (WPCN); (d) wirelessly powered backscatter communication (WPBC); (e) our proposed structure**

Power is transmitted through one link, information is transmitted through another link, and the power-collecting link provides power for the information-transmitting link, as shown in Fig. 1(c).

• Wirelessly powered backscatter communication (WPBC). Wireless power is transmitted through one link, and information is transmitted through another link. The backscatter modulation mechanism at the tag reflects and modulates the incoming radio frequency signal and sends it to the reader for communication. This kind of WPBC is widely used in RFID tags, which significantly improves the communication distance of wireless signals. Its disadvantage is that the power consumption of electrical appliances is required to be extremely low, and thus it cannot be widely used in other power scenarios, as shown in Fig. 1(d).

Relying on the three forms, many scholars have conducted in-depth studies. Researchers in the communication field have performed systematic research on the power ratio of energy and information and the modulation method of signals[11]. Researchers in the antenna field have designed various antennas and ports for wireless power transmission and communication, and fully considered the characteristics of port isolation[68] and frequency characteristics[69]. In this paper, we propose a new SWIPT structure, as shown in Fig. 1(e), by combining PMS and IoT applications. The electrical equipment in the IoT sends its position and power information to the FPGA on the transmitting end through sensors. After data processing, the FPGA will adaptively select the appropriate coding and generate the desired beams using PMS, according to the status of the electrical equipment in the external environment.

We propose a strategy to achieve the SWIPT system based on PMS, as illustrated in Fig. 2. When the battery of the electric device is low, its internal sensor will actively transmit position and energy information to the FPGA, and the PMS will supply energy to the sensor network that needs to be powered according to the coding of the FPGA. On the one hand, the PMS can form focused beams to transmit energy for the sensor network in the near-field region; on the other hand, the PMS will generate more efficient high-gain beams when the sensor network is in the far-field region. Through the internal communication between the sensor network and FPGA, the proposed system model enables the PMS to determine the charging target and select the appropriate charging scheme, which will solve the energy supply problem of the sensor network and significantly improve the system efficiency of SWIPT.

3 Adaptively Smart WPT Strategy Using PMS

In the WPT system, the most important thing is the transfer efficiency of the system. In different application scenarios, the power transmission beam has an important impact on efficiency. This paper aims to propose a method based on the location and power information of the device to be charged. PMS can intelligently allocate near-field focused

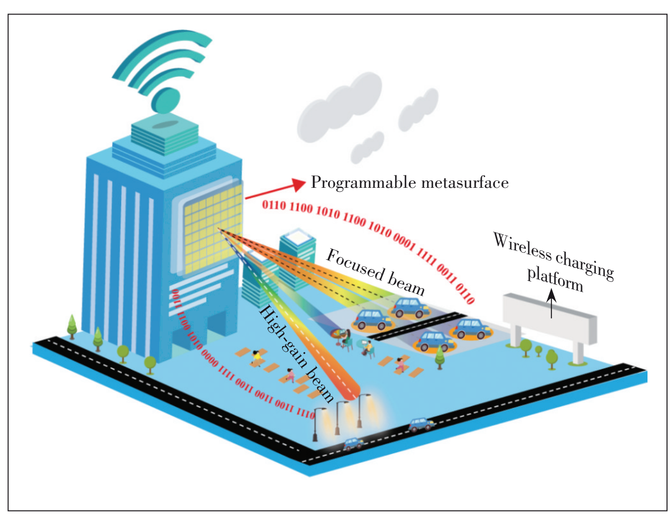

▲ **Figure 2. Application scenarios of the programmable metasurface (PMS) scheme for the simultaneous wireless information and power transfers (SWIPT) system** beams and far-field high-gain beams, which can achieve the purpose of efficient power transmission for different charging scenarios.

This system combines the designed PMS and IoT technology to form a new type of SWIPT system. As shown in Fig. 3, PMS can provide a flexible power beam for the device to be charged to improve the power transmission efficiency of the system. Taking the IoT network in the near field area as an example, the introduction of PMS will not affect the internal communication of the IoT network. It can also provide energy for the sensor nodes in the IoT network. When the battery energy of a sensor node is insufficient, it will actively send its energy and location information to the sensor connected to the FPGA.

After analyzing the data, the FPGA will control the switch of the corresponding PIN diodes and focus on the energy receiving part of the sensor node, which can meet the requirements of efficient and accurate energy transmission. It is also suitable for the far-field region. In summary, the proposed PMS model can simultaneously generate far-field high-gain beams and near-field focused beams. Combining PMS with the IoT networks with communication functions can achieve SWIPT, which enriches the design freedom of the power transmission system and greatly improves the power transmission efficiency of the entire system.

3.1 Far-Field WPT Strategy and Numerical Model

More and more attention has been paid to the realization of dynamic metasurfaces to construct advanced reconfigurable devices in recent years. In 2014, the concept of PMS was introduced to control the propagation of electromagnetic waves in a real-time programmable manner. Similar to the digital circuit technology, the different electromagnetic responses of the elements in the programmable metasurface are characterized by discrete digital codes. Therefore, the functional control of the far-field and the near-field can be realized by changing the digital code sequences.

Here, PMS is located on the plane, and each element can flexibly adjust the phase. A feed antenna is located above the PMS for spatial feeding. By tuning the active device on the programmable element, it can scan the far-field high-gain beam, find the target to be charged in the far-field, and supply power to it. The plane-wave angular spectrum (PWAS) method is used to describe the aperture radiation problem accurately. This method is derived from Fourier optics. When the tangential electric field on the PMS is known, it can be used to calculate the electric field distributions in the far-field and the near-field. According to the requirements of the WPT system for the field distribution, we can use the Fourier transform to decompose the required field distribution into a set of plane waves. The tangential electric field can determine these plane waves on the PMS. This method is also suitable for establishing a PMS far-field wireless energy transfer model. In this part, we will use PMS to generate a high-gain beam pattern capable of beam scanning. To generate the desired field distribution, the analysis of the far-field calculation using the PWAS method is shown in Fig. 4. During the analysis, we assume that the tangential electric fields of the two orthogonal E-field components $E_x^t(x, y)$ and $E_y^t(x, y)$ are known. PMS has $M \times M$ elements along the x-axis and y-axis, and the element size is $p_x \times p_y$. With these assumptions, we can obtain[70]

$$\vec{E}(x,y,z) = \int_{-\infty}^{\infty}\int_{-\infty}^{\infty}\left[\left(\hat{x} - \frac{u}{\gamma}\hat{z}\right)F_x(u,v) + \left(\hat{y} - \frac{v}{\gamma}\hat{z}\right) \times F_y(u,v)\right]\exp\left(-jk_0\vec{r}_p \cdot \vec{r}\right)\mathrm{d}u\mathrm{d}v, \tag{1}$$

where $F_x(u, v)$, and $F_y(u, v)$ are the spectrum functions for x- and y-directions, and k_0 is the free-space wave number. $\vec{r}_p$ represents the elemental position vector and $\vec{r}$ is the field vector.

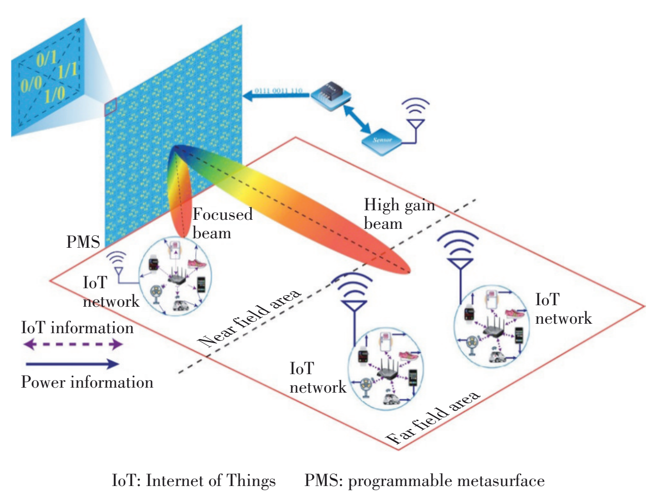

▲Figure 3. Application of PMS in the IoT network

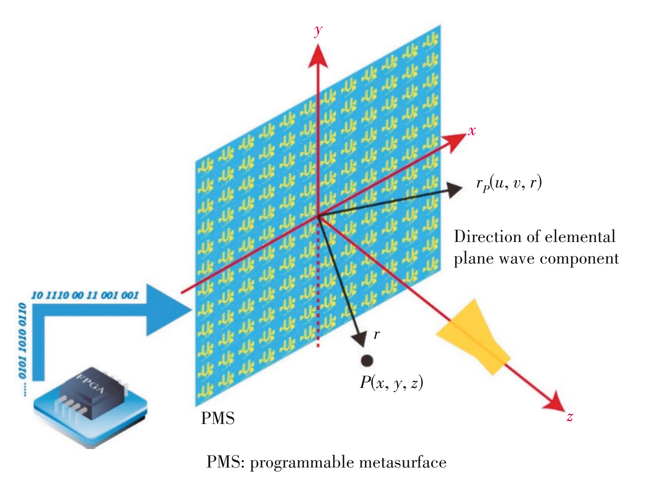

▲Figure 4. Configuration for far-field calculation using plane-wave angular spectrum (PWAS) approach

This equation can be calculated using the stationary phase method on the three directional components. Thus, we have

$$\vec{E}(x,y,z) \simeq j2\pi \frac{\exp(-jk_0 r)}{k_0 r}\left[(\gamma\hat{x} - u\hat{z})F_x(u,v) + (\gamma\hat{y} - v\hat{z})F_y(u,v)\right]. \tag{2}$$

In the spherical coordinate system, the above equation can be expressed as

$$\vec{E}(\theta,\varphi) \simeq j2\pi \frac{\exp(-jk_0 r)}{k_0 r}\cdot\left[(\cos\varphi\hat{\theta} - \cos\theta\sin\varphi\hat{\varphi})F_x(u,v) + (\sin\varphi\hat{\theta} + \cos\theta\cos\varphi\hat{\varphi})F_y(u,v)\right]. \tag{3}$$

Fourier transform can be used to describe the spectral functions

$$F_{x/y}(u,v) = \frac{1}{\lambda^2}\iint_{\text{surf}} E^t_{x/y}(x,y)\exp\left[jk_0(ux + vy)\right]\mathrm{d}x\mathrm{d}y, \tag{4}$$

where $u = \sin\theta\cos\phi$, and $v = \sin\theta\sin\phi$. This formula is used to express the integral on the surface of the PMS. In addition, because PMS is a periodic structure, we can calculate the result of an element and perform a summation calculation on it. We perform the coordinate conversion based on the above assumptions and analysis process. The specific expression is as follows.

$$x = x' + mp_x - \frac{(M-1)p_x}{2}, \quad m = 1,2,3,\ldots,M,$$
$$y = y' + np_y - \frac{(N-1)p_y}{2}, \quad n = 1,2,3,\ldots,N, \tag{5}$$

and

$$-\frac{p_x}{2} \leqslant x' \leqslant \frac{p_x}{2}, -\frac{p_y}{2} \leqslant y' \leqslant \frac{p_y}{2}. \tag{6}$$

Then, Eq. (4) can be rewritten as

$$F_{x/y}(u,v) = C\cdot\sum_{m=0}^{M-1}\sum_{n=0}^{N-1}\left[\exp\left[jk_0(ump_x + vnp_y)\right]\cdot I\right],$$

$$C = \frac{1}{\lambda^2}\exp\left\{-j\frac{k_0}{2}\left[u(M-1)p_x + v(N-1)p_y\right]\right\},$$

$$I = p_x p_y\,\mathrm{sinc}\left(\frac{k_0 u p_x}{2}\right)\mathrm{sinc}\left(\frac{k_0 v p_y}{2}\right)E^{m,n}_{x/y}(x_c,y_c), \tag{7}$$

where $E^{m,n}_{x/y}$ is the tangential E-field on each PMS element, and it can be expressed by

$$\begin{bmatrix} E_x^{m,n} \\ E_y^{m,n}\end{bmatrix} = \left[S^{m,n}_{TE,TM}\right]\begin{bmatrix} E_x^{inc} \\ E_y^{inc}\end{bmatrix}, \tag{8}$$

where $E^{inc}_{x/y}$ is the incident tangential electric field of the source, and $S^{m,n}_{TE,TM}$ is the element reflection coefficient which can be simulated with the full-wave simulator. To control the high-gain beam flexibly, we need to control the switch of the active devices on the PMS to produce a phase shift in each unit to form an equal wavefront phase in the desired area. The phase shift can be described as

$$\Phi(x_m,y_n) = -k_0(\sin\theta_0\cos\varphi_0 \times x_m + \sin\theta_0\sin\varphi_0 \times y_n) + k_0 d_{mn}, \tag{9}$$

where (θ_0, ϕ_0) is the beam pointing direction and d_{mn} is the distance from the feed horn to each element. For the digital coding PMS, Φ should be quantized[71]. When the phase shifts are calculated, the $S^{m,n}_{TE,TM}$ of each element is known. Therefore, far-field high-gain beams are generated when the distance from the PMS is greater than $2D^2/\lambda$, where λ is the wavelength and D is the largest dimension of the metasurface. The PMS radiation field can be calculated by Eqs. (3), (4), and (8).

According to the above theoretical analysis, through the PWAS mode calculation, a model with a frequency of 5.8 GHz is designed, as shown in Fig. 5. The PMS has 20×20 2-bit meta-atoms. Geometrical parameters are separately L_x = L_y = 30 mm, L_1 = 3.3 mm, L_2 = 2.6 mm, L_3 = 16.2 mm, w = 3 mm, and R_a = 4.5 mm. The entire array is printed on an F4B dielectric substrate with a thickness of 2 mm, the dielectric constant of which is 2.65, and the loss tangent angle is 0.005. The PIN diode model used is SMP1340. By combining the switchable states of the PIN diodes of low bits and high bits, the four states are termed as "00", "01", "10", and "11" respectively. The

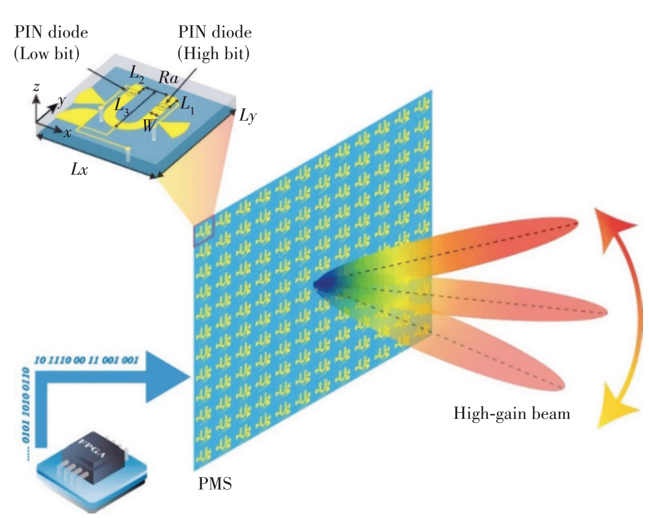

PMS: programmable metasurface

▲Figure 5. Schematic diagram of the high gain beam structure simulation results are shown in Fig. 6. We know that the phase differences of the four states are 90° at 5.8 GHz. The reflection amplitudes of "01" and "10" are close to −2 dB, and "00" and "11" states are less than 0.6 dB. The reason for this phenomenon may be that the two states of "01" and "10" work in a strong resonant mode, so their reflection amplitude fluctuates more obviously. Based on the above element model, we design a PMS array with 20×20 elements , which can realize beam scanning in the far-field area. Fig. 7 shows the coding patterns at 0°, 20°, and 40°, and the corresponding electric field distribution in the far-field area. To further verify the performance of the PMS array, we analyze its beam scanning characteristics, as shown in Fig. 8. It can be seen that there is a good scanning performance in the range of ±60°, which provides more favorable conditions for the wireless energy transmission.

3.2 Near-Field WPT Strategy and Numerical Model

A large number of studies have shown that when the target to be charged is in the near-field area of the antenna, the focused beam has higher power transfer efficiency. Through further analysis, it is concluded that the PWAS method is also suitable for calculating the electric field distribution in the near-

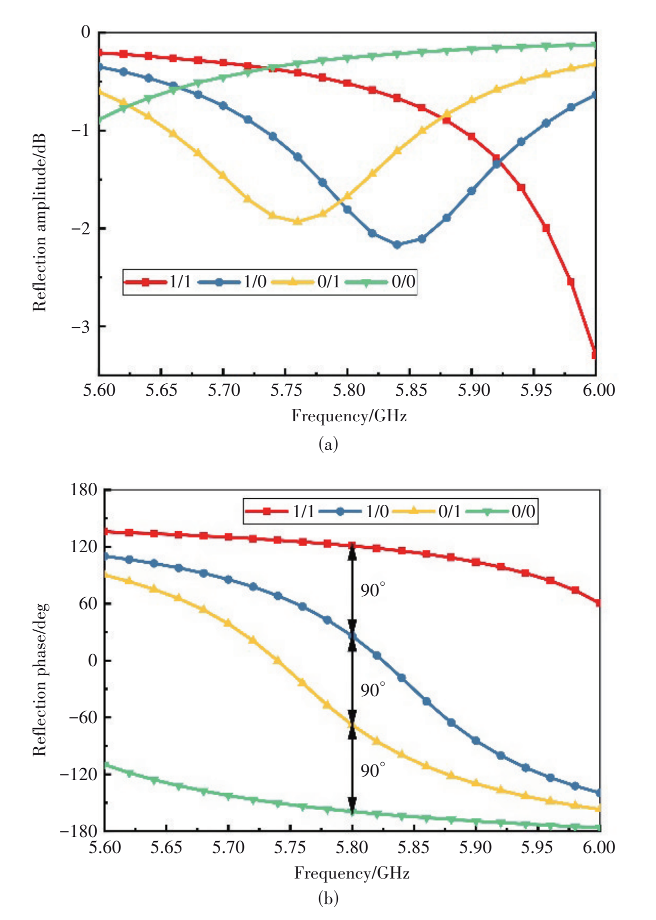

▲ Figure 6. Structure of the proposed 2-bit element: (a) reflection amplitude and (b) reflection phase

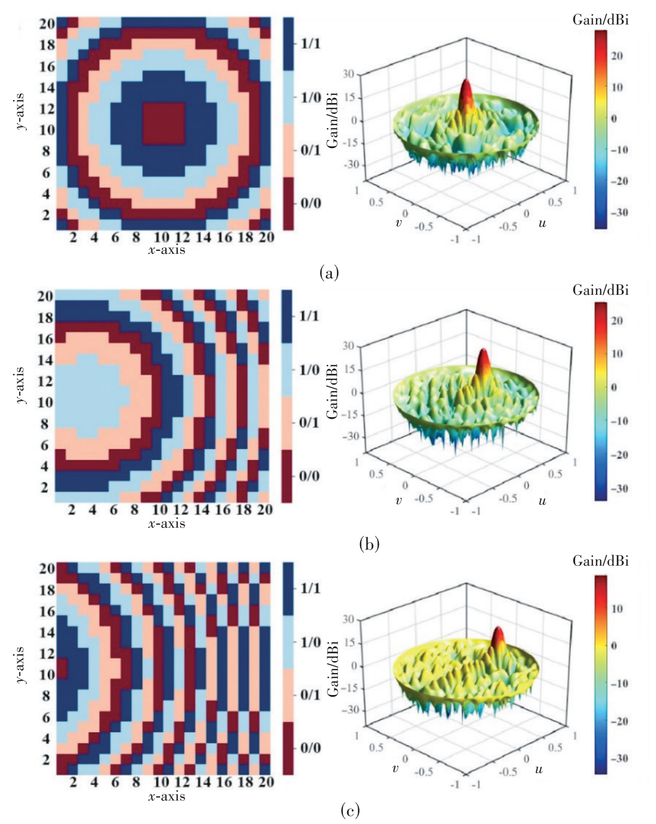

▲ Figure 7. Coding patterns and E-field distributions under different angles: (a) θ=0°, (b) θ=20° and, (c) θ=40°

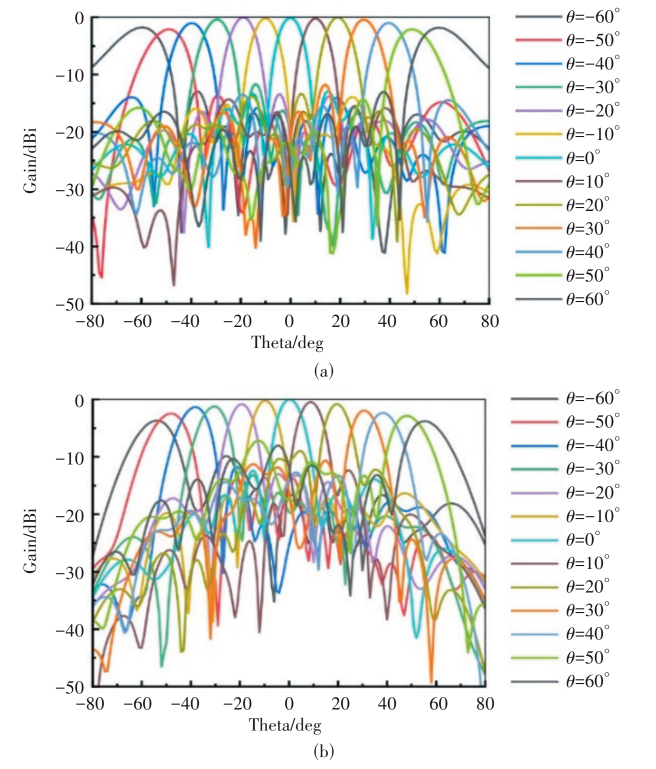

▲ Figure 8. Normalized radiation patterns of programmable metasurface (PMS): (a) E-plane beam-scanning and (b) H-plane beam-scanning field area. Fresnel diffraction theory is applied when the distance from the PMS is greater than $0.62\sqrt{D^3/\lambda}$ and less than $2D^2/\lambda$, and we can get the following approximate expression:

$$\gamma = \sqrt{1 - u^2 - v^2} \approx 1 - \frac{1}{2}(u^2 + v^2). \tag{10}$$

For the state of x polarization, we can use Eqs. (10) and (1) to get:

$$E_x = \exp(-jk_0 z)\int_{-\infty}^{\infty}\int_{-\infty}^{\infty} F_x(u,v)\exp\left[j\frac{k_0 z}{2}(u^2 + v^2)\right]\exp\left[-jk_0(xu + yv)\right]\mathrm{d}u\mathrm{d}v. \tag{11}$$

After the calculation using the two-dimensional convolution theorem, the integral of the above formula can be rewritten as:

$$E_x = \frac{j}{\lambda_z}\exp(-jk_0 z)\int_{-\infty}^{\infty}\int_{-\infty}^{\infty} E_x^t(u,v)\exp\left\{-\frac{jk_0}{2z}\left[(x-u)^2 + (y-u)^2\right]\right\}\mathrm{d}u\mathrm{d}v. \tag{12}$$

Eq. (12) can be discretized on every element of the PMS surface using Eqs. (5) and (6), resulting

$$E_x(x,y,z) = \frac{j}{2}\exp(-jk_0 z)\sum_{m=0}^{M-1}\sum_{n=0}^{N-1}\left\{\begin{array}{l} E_x^t(x_m,y_n)\cdot\left\{[C(t_2) - jS(t_2)] - [C(t_1) - jS(t_1)]\right\} \\ \cdot\left\{[C(t_2') - jS(t_2')] - [C(t_1') - jS(t_1')]\right\}\end{array}\right\}, \tag{13}$$

where

$$C(u) = \int_0^u \cos\left(\frac{\pi}{2}t^2\right)\mathrm{d}t, S(u) = \int_0^u \sin\left(\frac{\pi}{2}t^2\right)\mathrm{d}t$$

$$t_1 = \sqrt{\frac{k_0}{\pi z}}\left(\frac{p_x}{2} + x - mp_x + \frac{(M-1)p_x}{2}\right)$$

$$t_2 = \sqrt{\frac{k_0}{\pi z}}\left(-\frac{p_x}{2} + x - mp_x + \frac{(M-1)p_x}{2}\right)$$

$$t_1' = \sqrt{\frac{k_0}{\pi z}}\left(\frac{p_y}{2} + y - np_y + \frac{(N-1)p_y}{2}\right)$$

$$t_2' = \sqrt{\frac{k_0}{\pi z}}\left(-\frac{p_y}{2} + y - np_y + \frac{(N-1)p_y}{2}\right). \tag{14}$$

With these equations, we can analyze the electric field distribution in the near-field since the phase shift on each element is given.

To verify the validity of the near-field focusing formula of metasurfaces, the approximate solution of the Fresnel zone given by PWAS is used to design near-field electromagnetic energy focusing with metasurfaces. The designed model works at 5.8 GHz, and its element size is the same as the aforementioned high-gain beam antenna. The PMS is placed on the xoy plane and propagates along the z-axis, as shown in Fig. 9. According to Eq. (13), we have completed the flexible control of the focused beam, a dual-focus focused beam, and a single-focus focused beam at different positions. Figs. 10 (a), (d), (g) and (b), (e), (h) respectively show that the focus is at (0 m, 0 m, 0.5 m) and (0.2 m, 0.2 m, 0.5 m) of the coding patterns. The electric field distribution diagram of the PMS is at z = 0.5 m and on the xoz plane. The simulation data show that the PMS has a certain focus and scan functions, and the WPT system can supply power to charging equipment in different locations.

Figs. 10 (e), (f), and (i) describe the coding patterns of the dual focus (−0.2 m, −0.2 m, 0.5 m) and (0.2 m, 0.2 m, 0.5 m); their electric field distribution diagrams are at z=0.5 m and on the xoz plane, which indicates the PMS can supply power to multiple charging targets. Comprehensive analysis shows that the focused beam can converge most of the energy to one point, which meets our wireless power transmission requirements in the near-field area. It is worth pointing out that other quasi-non-diffraction beams, such as the Bessel beam and the Airy beam, can be flexibly regulated by PMS for wireless power transmission[72].

Because the size of the PMS in the simulation scheme is too large and inconvenient for processing, in order to verify the scheme's feasibility, we fabricate a PMS with 12×12 meta-atoms[48]. The size of PMS is 380 ×410 mm^2, as shown in Fig. 11(a). All DC biasing lines are led to the back of the

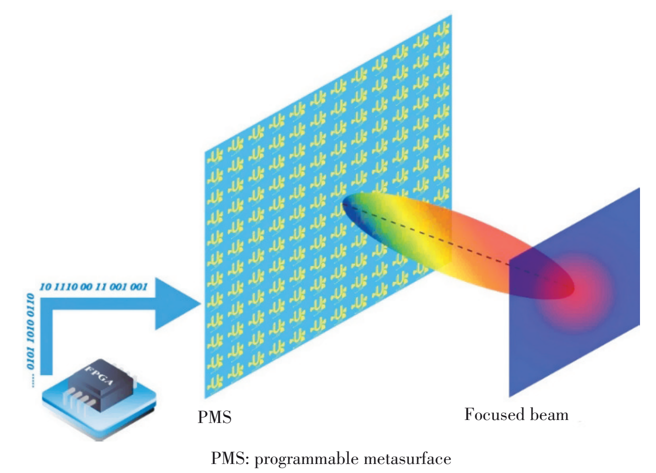

▲Figure 9. Schematic diagram of the focused beam in the near-field of PMS

PMS. The 144 biasing lines for the low bit or high bit are grouped into twelve 2×7 sockets, as shown in Fig. 11(b). There are twelve ports for the DC biasing lines and two grounding ports for each socket. The spots that can be controlled programmatically are measured in an anechoic chamber. The configuration of the measurement setup is shown in Fig. 11(c). For the convenience of observation, we normalize the electric field distribution obtained from the test. As shown in Fig. 12, all focal spots can be observed at the expected positions, indicating that the focal spot can be programmatically determined. It is fully proved that the scheme can solve the problem of multi-target WPT.

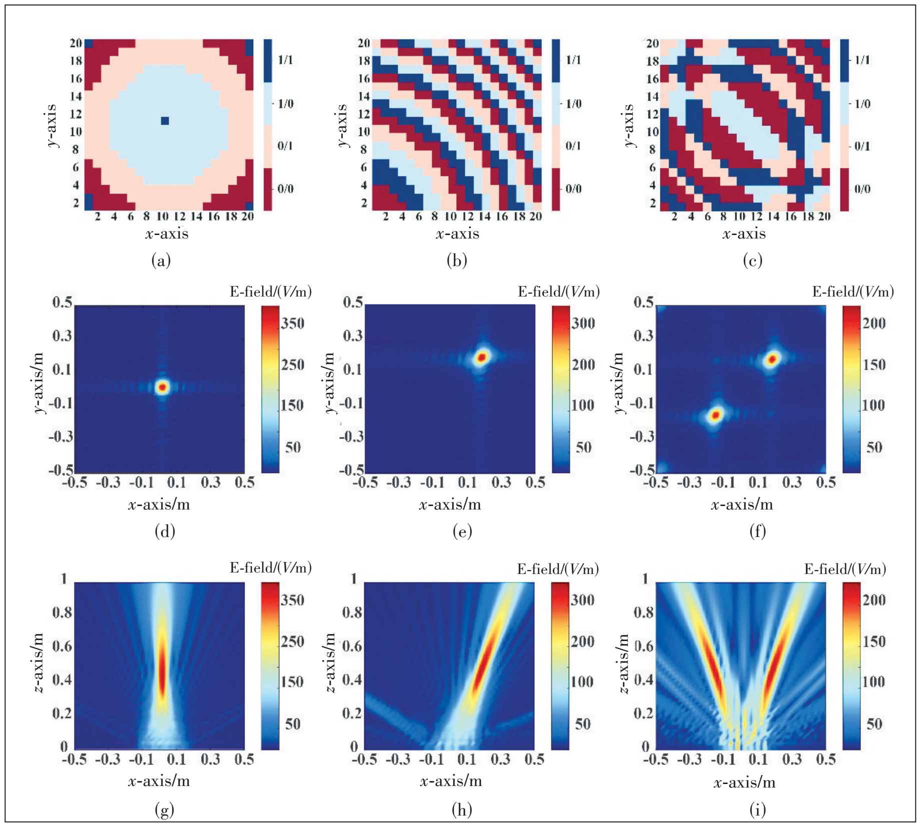

▲**Figure 10. Coding patterns and *E*-field distribution of the near-field focused beam, where (a), (d) and (g) describe the focus (0 m, 0 m, 0.5 m); (b), (e) and (h) describe the focus (0.2 m, 0.2 m, 0.5 m); (c), (f) and (i) describe the dual focus (0.2 m, 0.2 m, 0.5 m) and (−0.2 m, −0.2 m, 0.5 m)**

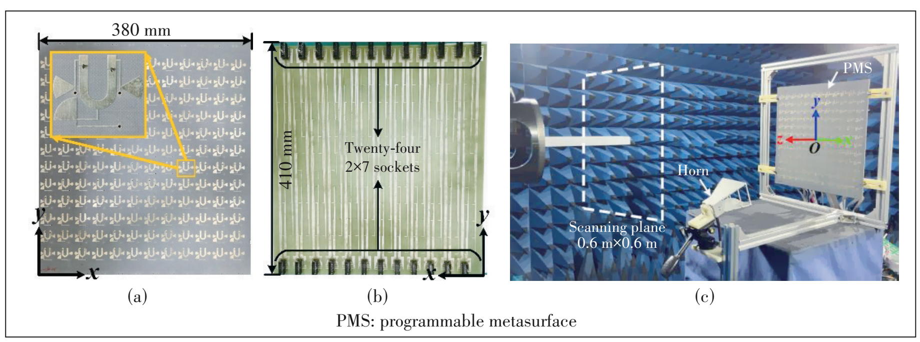

▲**Figure 11. Fabricated 2-bit PMS: (a) front view, (b) back view, and (c) near-field measurement scene for focal spots in the anechoic chamber**

4 WEH Metasurfaces and Transmission Efficiency Analyses

4.1 Design of Rectifying Metasurface

WEH is an important part of the SWIPT system. It is mainly composed of a receiving antenna and a rectifier circuit. After continuous exploration by many scientific researchers for the receiving antenna, many different types of receiving antennas have been proposed. Its compact structure, low sensitivity to the incident angle, polarization, and other characteristics have attracted wide attention[73–75], and it can meet the needs of WEH to a large extent. The main function of the rectifier circuit is to convert the RF energy captured by the receiving antenna into DC energy to provide usable energy for electrical equipment. To verify the feasibility of the strategy proposed in this paper, we propose a rectifying metasurface. First of all, we design a ring resonator with stubs. The operating frequency is 5.8 GHz. When the metasurface energy harvesting structure is designed, the Floquet port in ANSYS is used in conjunction with periodic boundary conditions to calculate the S parameters of the infinite period metasurface, energy harvesting efficiency, and other related parameters.

After simulation and optimization, we get the structure of the metasurface element, as shown in Fig. 13(a). The dielectric substrate used is F4B, the relative permittivity of which is 2.65, and the dielectric loss tangent is 0.001. The structure size is as follows: L_4=16 mm, W_1=0.53 mm, W_2=4.52 mm, W_3=0.57 mm, T=1 mm, and Load=430 Ω. A via is set on the diagonal of the element, and the energy collected by the metasurface is concentrated on the load, the radius of which is 0.2 mm. It is worth noting that we can flexibly design the working frequency and matching load of the metasurface by adjusting metasurface structure parameters. The harvesting efficiency of the metasurface can be calculated as[76]

$$\text{Efficiency} = \frac{P_L}{P_R} \times 100\%. \tag{15}$$

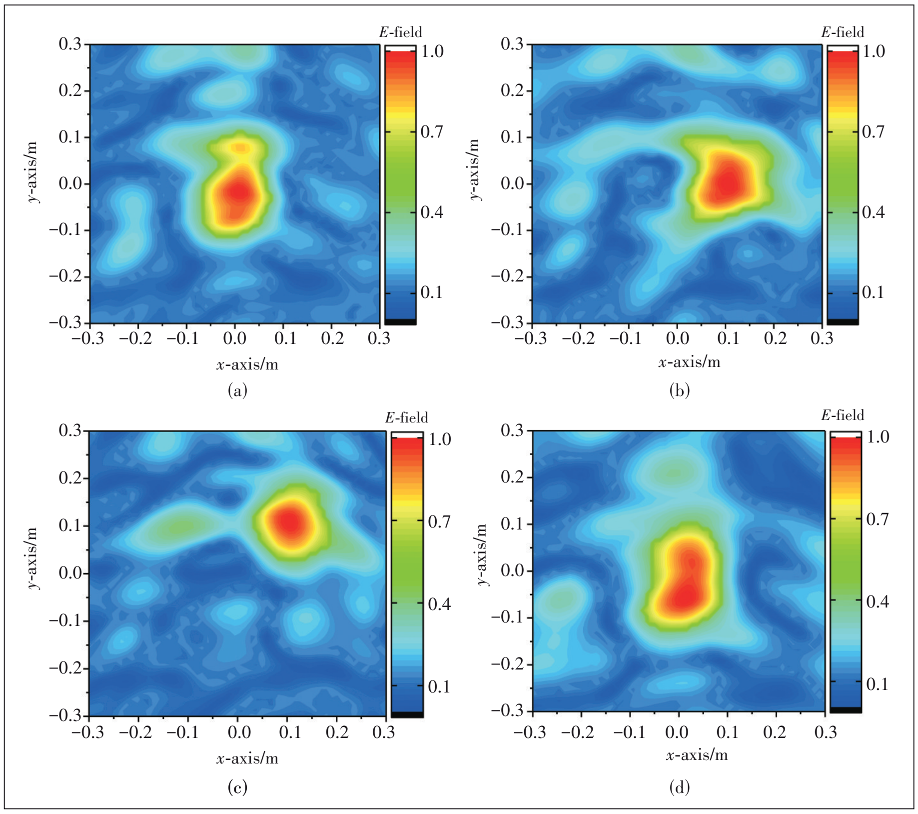

▲**Figure 12. Measured results of the focusing *E*-field distribution of the 2-bit PMS at (a) (0 m, 0 m, 0.75 m), (b) (0.1m, 0 m, 0.75 m), (c) (0.1 m, 0.1 m, 0.75 m), and (d) (0 m, 0 m, 0.9 m)**

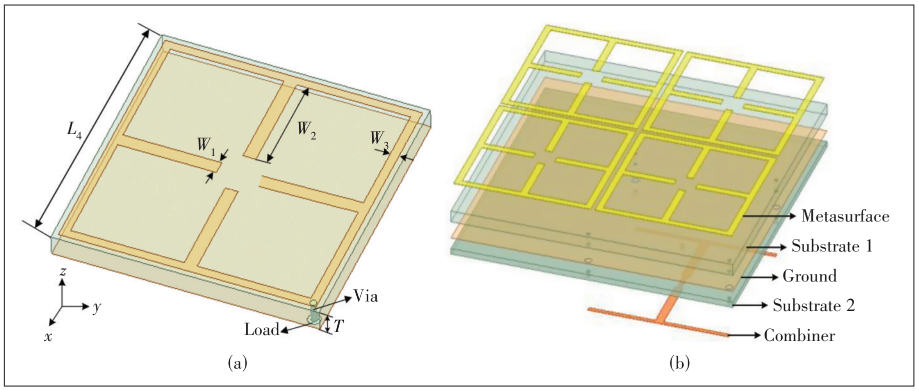

▲**Figure 13. Schematic diagram of metasurface structure: (a) element size and (b) array structure**

Among them, P_L is the energy collected by the load, and P_R is the energy incident on the metasurface, which can be obtained by integrating the Poynting vector along the incident direction on the metasurface. Fig. 14 shows the reflection coefficient $|S_{11}|$ of the metasurface and the harvesting efficiency of RF energy. It can be seen from the results that the impedance matching performance of the metasurface element is good at the operating frequency of 5.8 GHz; that is, the metasurface structure can capture electromagnetic wave energy. By calculating the received power of the lumped port, it can be seen that the RF energy harvesting efficiency of the metasurface energy harvester at 5.8 GHz can reach more than 90%. So we design a 2×2 metasurface array and converge four lumped ports into one port output through the combiner, which is convenient for subsequent combination with the rectifier circuit. The structure is shown in Fig. 13(b), which is divided into five layers in total. From the top to the bottom, the first layer is the metasurface array, the second layer is an F4B dielectric substrate, the third layer is ground, the fourth layer is an S7136 H dielectric substrate (relative permittivity is 3.55, and loss tangent is 0.004) with a thickness of 0.5 mm, and the fifth layer is a combiner. The whole structure can efficiently collect electromagnetic wave energy and output it through one port. To verify the incident angle and polarization stability of the metasurface structure, it is necessary to consider two cases of transverse electric (TE) and transverse magnetic (TM) oblique incidence. Fig. 15(a) shows the energy harvesting efficiency of TE polarization at different incident angles. When the incident angle is 0°, the maximum energy harvesting efficiency obtained at 5.8 GHz is 90%. When the incident angle is 30°, the maximum energy harvesting efficiency obtained at 5.9 GHz is 90%, and the energy harvesting efficiency at 5.8 GHz is 86%. When the incident angle is 60°, the maximum energy harvesting efficiency obtained at 6 GHz is 91%, and the energy collection efficiency at 5.8 GHz is 70%.

For TM polarization, as it is shown in Fig. 15(b), when the incident angles are 0°, 30°, and 60°, the MS will obtain the maximum energy collection efficiency at 5.8 GHz, 5.95 GHz, and 6.11 GHz, and their values are all near 90%. For 5.8 GHz, the energy harvesting efficiency of 30° and 60° oblique incidences is 83% and 74%, respectively. From the above analysis results, it can be seen that be it TE polarization or TM polarization, the working frequency of the maximum harvesting efficiency of the MS will shift as the incident angle increases. However, the energy harvesting efficiency at 5.8 GHz remains above 70%, showing good incident angle and polarization stability compared with traditional receiving antennas.

In order to convert the RF energy collected by the MS array into DC energy, we select MA4E1317 Schottky Barrier Diode

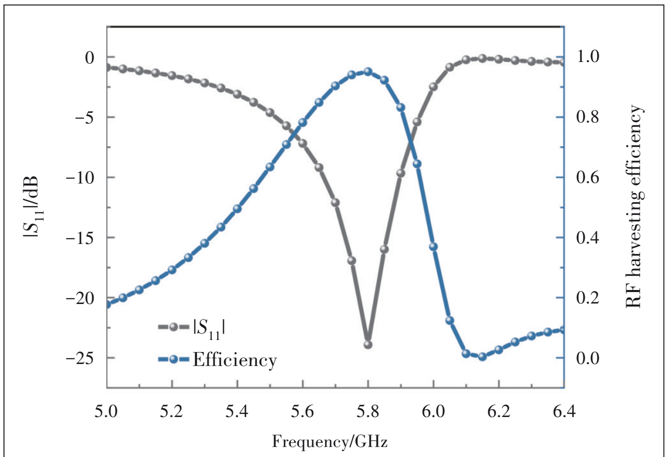

RF: radio frequency

▲Figure 14. $|S_{11}|$ and RF harvesting efficiency of the proposed metasurface element

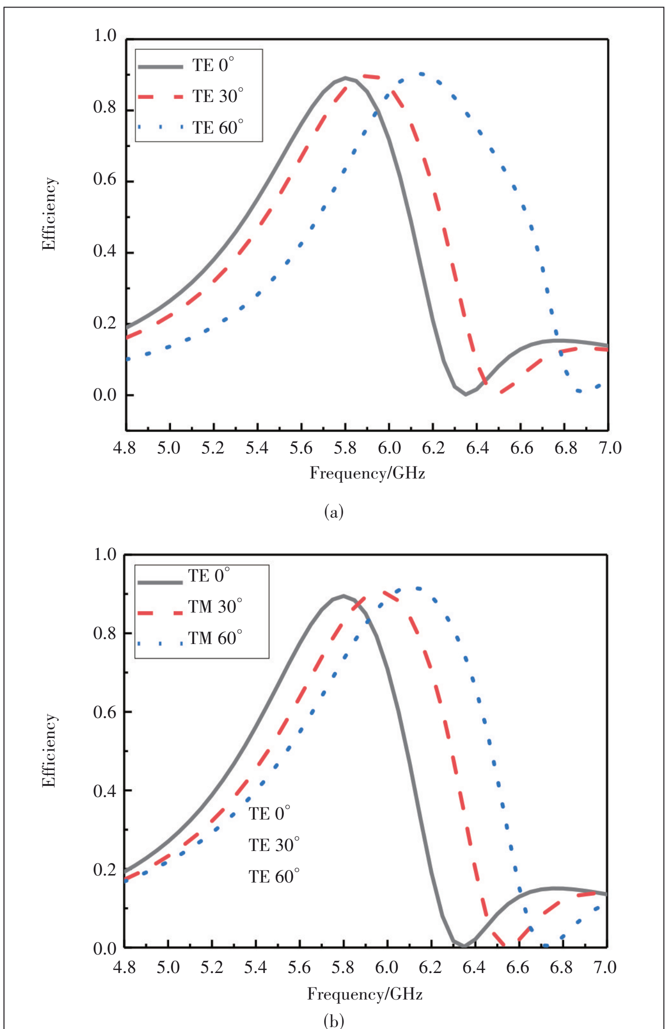

TE: transverse electric TM: transverse magnetic

▲Figure 15. Energy harvesting efficiency of metasurface: (a) TE polarization oblique incidence (0 – 60°), (b) TM polarization oblique incidence (0 – 60°)

(SBD) from MACOM as the rectifier device and designed an F-type rectifier circuit that works at 5.8 GHz. The selected dielectric substrate is the same as the dielectric substrate of the metasurface combiner in order to integrate the design with the MS array and reduce the cost. The size of the designed rectifier circuit is 25×15 mm^2, which is easy to integrate. The test and simulation performance are shown in Fig. 16. It can be found that when the input power is in the range of 12 dBm to 15 dBm, the rectification efficiency can be stabilized above 55%, and the output voltage at this time is higher than 1.6 V, which can provide energy for some low-power electrical appliances. In order to reduce the volume, we integrate the metasurface array and the rectifier circuit and process the principle prototype, as shown in Fig. 17, which can be used as the wireless energy harvesting part of the strategy we propose in this paper. Furthermore, a compact dual-band, wide-angle, and polarization-angle-independent rectifying metasurface can be applied for ambient energy harvesting[38].

4.2 Accurate WPT Efficiency Analysis of PMS

We accurately analyze the wireless power transmission efficiency from the near-field to far-field regions for the PMS. Fig. 18 shows the schematic diagram of the WPT system

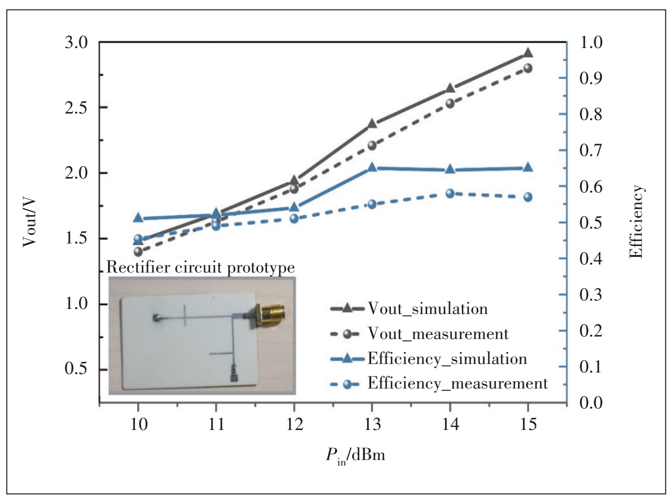

▲Figure 16. Rectifier circuit efficiency and output voltage

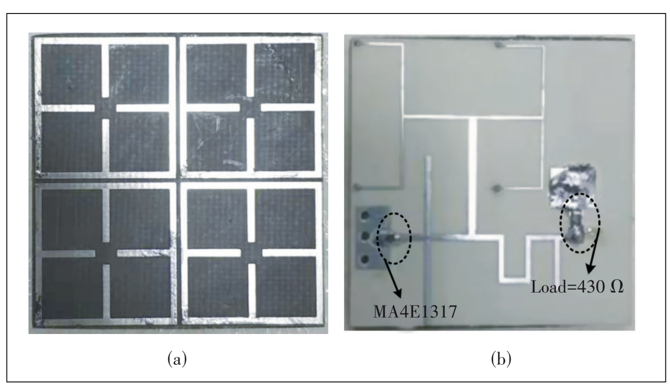

▲ Figure 17. A prototype of the rectifying metasurface: (a) front side and (b) backside

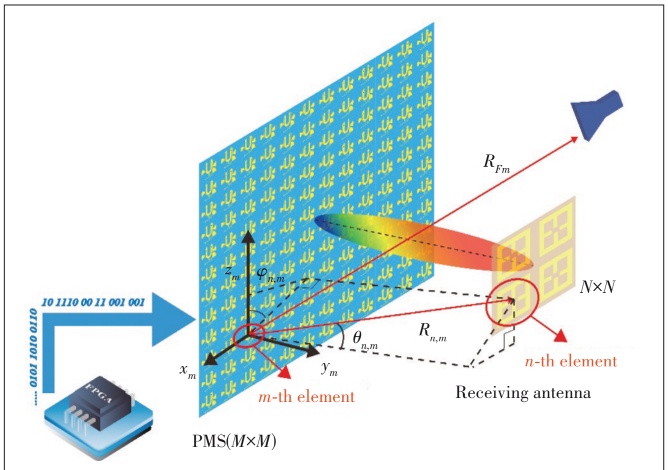

▲ **Figure 18. Schematic diagram of the wireless power transfer (WPT) system based on PMS and rectifying metasurface**

based on PMS. The transmitting part includes a feed horn and a PMS composed of $M\times M$=20×20 meta-atoms, and the receiving part is the $N\times N$=2×2 rectifying metasurface proposed in Section 4.1. The PMS is fed through a vertically incident horn antenna, and the transmitted power is P_T. The power of each element on the PMS can be extracted. Because the PMS is large enough, even if the receiving element is in the near field of the array, the receiving element is in the far field relative to the PMS element. Therefore, the energy received by the n-th receiving element from the m-th PMS element can be represented by Eq. (16). Where P_{sm} is the power of the m-th element of the PMS, λ is the wavelength. $G_{sm}(\theta_{n,m}, f_{n,m})$ and $G_{rn}(\theta_{m,n}, f_{m,n})$ are the gain of the m-th element of the PMS and the n-th element of the receiving antenna array, and $R_{n,m}$ is the distance between the two elements.

The power density can be expressed as $W = |E|^2/2\eta$. The amplitude of the electric field from the m-th element on the PMS to the n-th element of the receiving antenna array can be calculated by Eq. (17), where η is the wave impedance, k is the wavenumber, and $e^{-j(kR_{n,m}-\beta_m)}$ is the electric field phase. β_m is the initial phase of the PMS element which can be calculated by Eq. (18), where R_{Fm} is the distance from the phase center of the feed horn to the phase center of the PMS element, and β_{cm} is the compensation phase. According to the definition of power density, the power density received by the n-th receiving element from the m-th PMS element is $W_{n,m} = P_{rn,m}/(4\pi R_{n,m}^{\ 2})$[77]. Assuming that the radiation source is isotropic, the power generated at R distance from the power source is $P = 4\pi R^2 W = 4\pi R^2|E|^2/2\eta$. Eq. (19) can calculate the power received by the n-th receiving element from the entire PMS. The total power P_R received by the receiving antenna is the superposition of the power of each receiving element. The wireless power transmission efficiency is defined as the ratio of the total power received by the receiving antenna array to the microwave power emitted by the feed horn, as shown in Eq. (21).

It is worth noting that the PMS proposed in this paper introduces insertion loss due to the PIN diodes, which mainly affects the gain of antennas, so Eq. (21) is also applicable to the efficiency calculation of the PMS.

$$P_{r_{n,m}} = P_{s_m} G_{s_m}(\theta_{n,m},\phi_{n,m}) G_{r_n}(\theta_{m,n},\phi_{m,n}) \left(\frac{\lambda}{4\pi R_{n,m}}\right)^2. \tag{16}$$

$$E_{n,m} = \sqrt{2\eta W_{n,m}}\, e^{-j(kR_{n,m} - \beta_m)}. \tag{17}$$

$$\beta_m = \beta_{c_m}(l) - kR_{F_m}. \tag{18}$$

$$P_{r_n} = \frac{4\pi}{2\eta}\left|\sum_{m=1}^{M} R_{n,m} E_{n,m}\right|^2 = \left(\frac{\lambda}{4\pi}\right)^2 \left|\sum_{m=1}^{M} \sqrt{P_{s_m} G_{s_m}(\theta_{n,m},\phi_{n,m}) G_{r_n}(\theta_{n,m},-\phi_{n,m})}\, \frac{e^{-j(kR_{n,m} - \beta_{c_m}(l) + kR_{F_m})}}{R_{n,m}}\right|^2. \tag{19}$$

$$P_R = \left(\frac{\lambda}{4\pi}\right)^2 \left(\sum_{n=1}^{N}\left|\sum_{m=1}^{M} \sqrt{P_{s_m} G_{s_m}(\theta_{n,m},\phi_{n,m}) G_{r_n}(\theta_{n,m},-\phi_{n,m})}\, \frac{e^{-j(kR_{n,m} - \beta_{c_m}(l) + kR_{F_m})}}{R_{n,m}}\right|^2\right). \tag{20}$$

$$\frac{P_R}{P_T} = \left(\frac{\lambda}{4\pi}\right)^2 \frac{\left(\sum_{n=1}^{N}\left|\sum_{m=1}^{M} \sqrt{P_{s_m} G_{s_m}(\theta_{n,m},\phi_{n,m}) G_{r_n}(\theta_{n,m},-\phi_{n,m})}\, \frac{e^{-j(kR_{n,m} - \beta_{c_m}(l) + kR_{F_m})}}{R_{n,m}}\right|^2\right)}{P_T}. \tag{21}$$

For the WPT system composed of PMS, we analyze the transmission efficiency of the beams mentioned in Sections 3.1 and 3.2. Fig. 19 shows the efficiency comparison of different beams when propagating along the center of the PMS. For focused beams, we can see from the figure that the transmission efficiency at our preset focal point (0 m, 0 m, 0.5 m) is higher than 25% and much higher than the transmission efficiency of the high-gain beam. But as the transmission distance increases or decreases, the transmission efficiency of the focused beam will drop sharply. This can be solved by the strategy mentioned in this paper, which is to achieve precise positioning by transmitting location information. When the distance between the receiving metasurface array and the PMS is greater than 1 m, the advantages of the high-gain beam are gradually revealed. Its transmission efficiency is greater than that of the focused beam, suitable for long-distance wireless

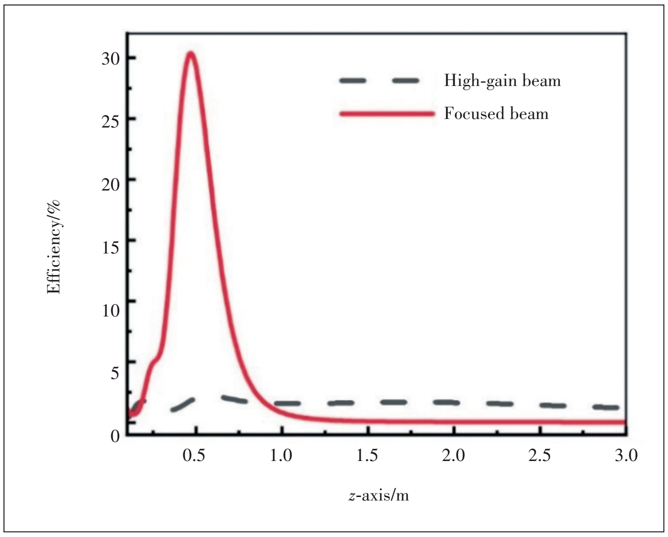

▲Figure 19. Wireless power transmission efficiency versus distance using high-gain beam and focused beam

power transmission. Based on the above analysis results, it can be obtained that the high-gain beam is suitable for the far-field WPT system, and the focused beam is suitable for the near-field WPT system. It fully demonstrates the feasibility of the strategy proposed in this paper.

5 Future Work and Conclusions

In previous sections, we describe a new strategy for the SWIPT system using the advanced metamaterials, PMS, including the overall solution scheme, the adaptively smart WPT strategy, WEH metasurfaces, and wireless power transmission efficiency analyses. We emphasize that the WPT and WEH using PMS are the major topics of this work because of the information that PMSs have been deeply studied. When the two aspects are properly unified, a feasible SWIPT solution to the self-sustainable 6G network may be realized. In this section, we discuss future research directions of the SWIPT network based on the PMS solution scheme, and make a systematic conclusion of this paper.

5.1 Full-Duplex PMS

A typical PMS could operate the amplitude, phase, and polarization of the incident EM waves. Technically, PMS is suitable for changing the channel state, which cannot be used to enhance the communication capacity. Researchers are aware of this and some RF channel operational PMSs have been reported[78–80]. The concept and prototype of multiple-input multiple-output (MIMO) PMS were proposed and tested[81]. Besides, a novel holographic MIMO surface was envisioned for the 6G network[82]. A theoretical analysis of dynamic metasurface antennas for uplink massive MIMO systems was presented in Ref. [83]. However, a complete uplink and downlink experiment based on PMS is still unavailable. Thus, realizing a full-duplex PMS would be the major research direction in the future.

5.2 Wireless Information and Power Integrated Surface

Imposing WPT and WEH techniques presented in this paper on the full-duplex PMS, we have a wireless information and power integrated surface (WIPIS), which is our main solution scheme to the SWIPT network. Distinct from the existing SWIPT, the WIPIS scheme depends on a cutting-edge technique, PMS. Both the information modulation and power management implemented by such a paradigm will gain more attention in microwave techniques, antenna propagation, and wireless communication communities. Although great efforts have been put into the WIPIS prototype design and modeling, it is still at the early stage. In the foreseeable future, we believe that the WIPIS-based system would appear. Recent advances in metamaterials and metasurfaces can stimulate the research for simultaneous wireless information and power transmission[84–87].

5.3 Base Station Side, Relay Side, and Edge Side WIPIS

For different working scenarios, the WIPIS should provide distinct functionalities. A three-layer architecture of a WIPIS-based network is envisioned, including the base station side, the relay side, and the edge side. On the base station side, a WIPIS base station could offer point-to-point, point-to-multipoint, and specific area power coverage services in addition to mobile network access. On the relay side, a WIPIS could operate as a repeater or improve the channels. Besides, the relay WIPIS redistributes wireless power to surrounding IoT sensors or the edge side WIPIS. We emphasize that the main energy for a relay WIPIS is guaranteed by the WIPIS base station. At the edge side, microwatt level devices are accompanied by the low-level WIPISs which connect the relay WIPIS and coordinate the energy interconnections. All these WIPISs collaborate to form a featured SWIPT wireless network.

5.4 Conclusions

A perspective strategy of using PMS for the SWIPT system is proposed. Based on the PMS hardware platform, we develop an adaptively smart WPT strategy including the numerical models and analysis results of the near-field and far-field WPT systems. To collect and capture the wireless powers, the rectifying metasurface is presented employing the WEH technique. More importantly, the wireless power transmission efficiency is analyzed when using PMS as the transmitter and the rectifying metasurface as the receiver, suggesting that the proposed PMS-based SWIPT network is efficient and low-cost. The future research directions using the proposed scheme are summarized. The opportunities and challenges co-exist for implementing the future SWIPT network that can fulfill the carbon peak and carbon neutralization development strategy.

References

[1] ANDREWS J G, BUZZI S, CHOI W, et al., What will 5G be [J]. IEEE journal on selected areas in communications, 2014, 32(6): 1065 – 1082. DOI: 10.1109/JSAC.2014.2328098

[2] HU R Q, QIAN Y. An energy efficient and spectrum efficient wireless heterogeneous network framework for 5G systems [J]. IEEE communications magazine, 2014, 52(5): 94 – 101. DOI: 10.1109/mcom.2014.6815898

[3] AL-FUQAHA A, GUIZANI M, MOHAMMADI M, et al. Internet of Things: a survey on enabling technologies, protocols, and applications [J]. IEEE communications surveys & tutorials, 2015, 17(4): 2347 – 2376. DOI: 10.1109/COMST.2015.2444095

[4] VARSHNEY L R. Transporting information and energy simultaneously [C]//Proceedings of 2008 IEEE International Symposium on Information Theory. IEEE, 2008: 1612 – 1616. DOI: 10.1109/ISIT.2008.4595260

[5] PONNIMBADUGE P T D, JAYAKODY D N K, SHARMA S K, et al. Simultaneous wireless information and power transfer (SWIPT): recent advances and future challenges [J]. IEEE communications surveys & tutorials, 2018, 20(1): 264 – 302. DOI: 10.1109/COMST.2017.2783901

[6] CLERCKX B, ZHANG R, SCHOBER R, et al. Fundamentals of wireless information and power transfer: from RF energy harvester models to signal and system designs [J]. IEEE journal on selected areas in communications, 2019, 37(1): 4 – 33. DOI: 10.1109/JSAC.2018.2872615

[7] ZHANG R, HO C K. MIMO broadcasting for simultaneous wireless information and power transfer [J]. IEEE transactions on wireless communications, 2013, 12(5): 1989 – 2001. DOI: 10.1109/TWC.2013.031813.120224

[8] HUANG K B, LARSSON E G. Simultaneous information-and-power transfer for broadband downlink systems [C]//IEEE International Conference on Acoustics, Speech and Signal Processing. IEEE, 2013. DOI: 10.1109/ICASSP.2013.6638500

[9] DIAMANTOULAKIS P D, KARAGIANNIDIS G K, DING Z G. Simultaneous lightwave information and power transfer (SLIPT) [J]. IEEE transactions on green communications and networking, 2018, 2(3): 764 – 773. DOI: 10.1109/TGCN.2018.2818325

[10] DO T P, SONG I, KIM Y H. Simultaneous wireless transfer of power and information in a decode-and-forward two-way relaying network [J]. IEEE transactions on wireless communications, 2017, 16(3): 1579 – 1592. DOI: 10.1109/TWC.2017.2648801

[11] ZHOU X, ZHANG R, HO C K. Wireless information and power transfer: architecture design and rate-energy tradeoff [J]. IEEE transactions on communications, 2013, 61(11): 4754 – 4767. DOI: 10.1109/TCOMM.2013.13.120855

[12] KRIKIDIS I, TIMOTHEOU S, NIKOLAOU S, et al. Simultaneous wireless information and power transfer in modern communication systems [J]. IEEE communications magazine, 2014, 52(11): 104 – 110. DOI: 10.1109/MCOM.2014.6957150

[13] CHEN H, LI Y H, JIANG Y X, et al. Distributed power splitting for SWIPT in relay interference channels using game theory [J]. IEEE transactions on wireless communications, 2015, 14(1): 410 – 420. DOI: 10.1109/TWC.2014.2349892

[14] KHAN T A, ALKHATEEB A, HEATH R W. Millimeter wave energy harvesting [J]. IEEE transactions on wireless communications, 2016, 15(9): 6048 – 6062. DOI: 10.1109/TWC.2016.2577582

[15] XIA M H, AISSA S. On the efficiency of far-field wireless power transfer [J]. IEEE transactions on signal processing, 2015, 63(11): 2835 – 2847. DOI: 10.1109/TSP.2015.2417497

[16] LIU H W, KIM K J, KWAK K S, et al. Power splitting-based SWIPT with decode-and-forward full-duplex relaying [J]. IEEE transactions on wireless communications, 2016, 15(11): 7561 – 7577. DOI: 10.1109/TWC.2016.2604801

[17] LU X, WANG P, NIYATO D, et al. Wireless charging technologies: Fundamentals, standards, and network applications [J]. IEEE communications surveys & tutorials, 2016, 18(2): 1413 – 1452. DOI: 10.1109/COMST.2015.2499783

[18] NG D W K, LO E S, SCHOBER R. Wireless information and power transfer: energy efficiency optimization in OFDMA systems [J]. IEEE transactions on wireless communications, 2013, 12(12): 6352 – 6370. DOI: 10.1109/TWC.2013.103113.130470

[19] KURS A, KARALIS A, MOFFATT R, et al. Wireless power transfer via strongly coupled magnetic resonances [J]. Science, 2007, 317(5834): 83 – 86. DOI: 10.1126/science.1143254

[20] MAYORDOMO I, DRÄGER T, SPIES P, et al. An overview of technical challenges and advances of inductive wireless power transmission [J]. Proceedings of the IEEE, 2013, 101(6): 1302 – 1311. DOI: 10.1109/JPROC.2013.2243691

[21] COVIC G A, BOYS J T. Inductive power transfer [J]. Proceedings of the IEEE, 2013, 101(6): 1276 – 1289. DOI: 10.1109/JPROC.2013.2244536

[22] ZHANG Z, PANG H L, GEORGIADIS A, et al. Wireless power transfer: an overview [J]. IEEE transactions on industrial electronics, 2019, 66(2): 1044 – 1058. DOI: 10.1109/TIE.2018.2835378

[23] HUI S Y R, ZHONG W X, LEE C K. A critical review of recent progress in mid-range wireless power transfer [J]. IEEE transactions on power electronics, 2014, 29(9): 4500 – 4511. DOI: 10.1109/TPEL.2013.2249670

[24] BROWN W C. The history of power transmission by radio waves [J]. IEEE transactions on microwave theory and techniques, 1984, 32(9): 1230 – 1242. DOI: 10.1109/TMTT.1984.1132833

[25] BROWN W C. Status of the microwave power transmission components for the solar power satellite [J]. IEEE transactions on microwave theory and techniques, 1981, 29(12): 1319 – 1327. DOI: 10.1109/TMTT.1981.1130559

[26] SHINOHARA N. History and innovation of wireless power transfer via microwaves [J]. IEEE journal of microwaves, 2021, 1(1): 218 – 228. DOI: 10.1109/JMW.2020.3030896

[27] YANG B, CHEN X J, CHU J, et al. A 5.8-GHz phased array system using power-variable phase-controlled magnetrons for wireless power transfer [J]. IEEE transactions on microwave theory and techniques, 2020, 68(11): 4951 – 4959. DOI: 10.1109/TMTT.2020.3007187

[28] RODENBECK C T, JAFFE P I, STRASSNER B H, et al. Microwave and millimeter wave power beaming [J]. IEEE journal of microwaves, 2021, 1(1): 229 – 259. DOI: 10.1109/jmw.2020.3033992

[29] SHINOHARA N. Trends in wireless power transfer: WPT technology for energy harvesting, mllimeter-wave/THz rectennas, MIMO-WPT, and advances in near-field WPT applications [J]. IEEE microwave magazine, 2021, 22(1): 46 – 59. DOI: 10.1109/MMM.2020.3027935

[30] TAKABAYASHI N, SHINOHARA N, MITANI T, et al. Rectification improvement with flat-topped beams on 2.45-GHz rectenna arrays [J]. IEEE transactions on microwave theory and techniques, 2020, 68(3): 1151 – 1163. DOI: 10.1109/TMTT.2019.2951098

[31] WANG C, YANG B, SHINOHARA N. Study and design of a 2.45-GHz rectifier achieving 91% efficiency at 5-W input power [J]. IEEE microwave and wireless components letters, 2021, 31(1): 76 – 79. DOI: 10.1109/LMWC.2020.3032574

[32] CUI T J, SMITH D, LIU R P, et al. Metamaterials: theory, design and applications [M]. Heidelberg, Germany: Springer, 2010. DOI: 10.1007/978-1-4419-0573-4

[33] YU N F, GENEVET P, KATS M A, et al. Light propagation with phase discontinuities: generalized laws of reflection and refraction [J]. Science, 2011, 334(6054): 333 – 337. DOI: 10.1126/science.1210713

[34] YU N, CAPASSO F. Flat optics with designer metasurfaces [J]. Nature materials, 2014, 13 (2): 139 – 150. DOI: 10.1038/nmat3839

[35] LIU R, JI C, MOCK J J, et al. Braodband groud-plane cloack [J]. Science, 2009, 323(5912): 336 – 369. DOI: 10.1126/science.1166949

[36] ZHOU J F, ZHANG P, HAN J Q, et al. Metamaterials and metasurfaces for wireless power transfer and energy harvesting [J]. Proceedings of the IEEE, 2022, 110(1): 31 – 55. DOI: 10.1109/JPROC.2021.3127493

[37] LI L, ZHANG P, CHENG F J, et al. An optically transparent near-field focusing metasurface [J]. IEEE transactions on microwave theory and techniques, 2021, 69(4): 2015 – 2027. DOI: 10.1109/TMTT.2021.3061475

[38] LI L, ZHANG X M, SONG C Y, et al. Compact dual-band, wide-angle, polarization- angle-independent rectifying metasurface for ambient energy harvesting and wireless power transfer [J]. IEEE transactions on microwave theory and techniques, 2021, 69(3): 1518 – 1528. DOI: 10.1109/TMTT.2020.3040962

[39] LI L, ZHANG X M, SONG C Y, et al. Progress, challenges, and perspective on metasurfaces for ambient radio frequency energy harvesting [J]. Applied physics letters, 2020, 116(6): 060501. DOI: 10.1063/1.5140966

[40] ERKMEN F, ALMONEEF T S, RAMAHI O M. Scalable electromagnetic energy harvesting using frequency-selective surfaces [J]. IEEE transactions on microwave theory and techniques, 2018, 66(5): 2433 – 2441. DOI: 10.1109/TMTT.2018.2804956

[41] ALMONEEF T S, RAMAHI O M. Metamaterial electromagnetic energy harvester with near unity efficiency [J]. Applied physics letters, 2015, 106(15): 153902. DOI: 10.1063/1.4916232

[42] ZHANG X M, LIU H X, LI L. Tri-band miniaturized wide-angle and polarization-insensitive metasurface for ambient energy harvesting [J]. Applied physics letters, 2017, 111(7): 071902. DOI: 10.1063/1.4999327
[43] ALAVIKIA B, ALMONEEF T S, RAMAHI O M. Wideband resonator arrays for electromagnetic energy harvesting and wireless power transfer [J]. Applied physics letters, 2015, 107(24): 243902. DOI: 10.1063/1.4937591
[44] ZHANG P, YI H, LIU H X, et al. Back-to-back microstrip antenna design for broadband wide-angle RF energy harvesting and dedicated wireless power transfer [J]. IEEE access, 2020, 8: 126868 – 126875. DOI: 10.1109/ACCESS.2020.3008551
[45] ZHANG P, LI L, ZHANG X M, et al. Design, measurement and analysis of near-field focusing reflective metasurface for dual-polarization and multi-focus wireless power transfer [J]. IEEE access, 2019, 7: 110387 – 110399. DOI: 10.1109/ACCESS.2019.2934135
[46] YU S X, LIU H X, LI L. Design of near-field focused metasurface for high-efficient wireless power transfer with multifocus characteristics [J]. IEEE transactions on industrial electronics, 2019, 66(5): 3993 – 4002. DOI: 10.1109/TIE.2018.2815991
[47] CUI T J, QI M Q, WAN X, et al. Coding metamaterials, digital metamaterials and programmable metamaterials [J]. Light: science & applications, 2014, 3(10): 218. DOI: 10.1038/lsa.2014.99
[48] HAN J Q, LI L, MA X J, et al. Adaptively smart wireless power transfer using 2-bit programmable metasurface [J]. IEEE transactions on industrial electronics, 2022, 69(8): 8524 – 8534. DOI: 10.1109/TIE.2021.3105988
[49] DAI J Y, TANG W K, CHEN M Z, et al. Wireless communication based on information metasurfaces [J]. IEEE transactions on microwave theory and techniques, 2021, 69(3): 1493 – 1510. DOI: 10.1109/TMTT.2021.3054662
[50] ZHANG L, CHEN X Q, LIU S, et al. Space-time-coding digital metasurfaces [J]. Nature communications, 2018, 9: 4334. DOI: 10.1038/s41467-018-06802-0
[51] ZHANG L, CUI T J. Space-time-coding digital metasurfaces: principles and applications [J]. Research, 2021: 1 – 25. DOI: 10.34133/2021/9802673
[52] WU H T, BAI G D, LIU S, et al. Information theory of metasurfaces [J]. National science review, 2020, 7(3): 561 – 571. DOI: 10.1093/nsr/nwz195
[53] CUI T J, LI L L, LIU S, et al. Information metamaterial systems [J]. IScience, 2020, 23(8): 101403. DOI: 10.1016/j.isci.2020.101403
[54] MA Q, CUI T J. Information Metamaterials: Bridging the physical world and digital world [J]. PhotoniX, 2020, 1: 1. DOI: 10.1186/s43074-020-00006-w
[55] ZHANG L, CHEN M Z, TANG W K, et al. A wireless communication scheme based on space- and frequency-division multiplexing using digital metasurfaces [J]. Nature electronics, 2021, 4(3): 218 – 227. DOI: 10.1038/s41928-021-00554-4
[56] TANG W K, DAI J Y, CHEN M Z, et al. MIMO transmission through reconfigurable intelligent surface: System design, analysis, and implementation [J]. IEEE journal on selected areas in communications, 2020, 38(11): 2683 – 2699. DOI: 10.1109/JSAC.2020.3007055
[57] CHEN M Z, TANG W K, DAI J Y, et al. Accurate and broadband manipulations of harmonic amplitudes and phases to reach 256 QAM millimeter-wave wireless communications by time-domain digital coding metasurface [J]. National science review, 2021, 9(1): 134. DOI: 10.1093/nsr/nwab134
[58] WU H, GAO X X, ZHANG L, et al. Harmonic information transitions of spatiotemporal metasurfaces [J]. Light: science & applications, 2020, 9: 198. DOI: 10.1038/s41377-020-00441-1
[59] ZHAO H T, SHUANG Y, WEI M L, et al. Metasurface-assisted massive backscatter wireless communication with commodity Wi-Fi signals [J]. Nature communications, 2020, 11: 3926. DOI: 10.1038/s41467-020-17808-y
[60] RUAN H X, LI L L. Imaging resolution analysis of single-frequency and single-sensor programmable microwave imager [J]. IEEE transactions on antennas and propagation, 2020, 68(11): 7727 – 7732. DOI: 10.1109/TAP.2020.2986653
[61] LI L, SHUANG Y, MA Q, et al. Intelligent metasurface imager and recognizer [J]. Light: science & applications, 2019, 8: 97. DOI: 10.1038/s41377-019-0209-z
[62] MA Q, BAI G D, JING H B, et al. Smart metasurface with self-adaptively reprogrammable functions [J]. Light: science & applications, 2019, 8: 98. DOI: 10.1038/s41377-019-0205-3
[63] LI L L, RUAN H X, LIU C, et al. Machine-learning reprogrammable metasurface imager [J]. Nature communications, 2019, 10(1): 1082. DOI: 10.1038/s41467-019-09103-2
[64] HUANG T J, TANG H H, TAN Y H, et al. Terahertz super-resolution imaging based on subwavelength metallic grating [J]. IEEE transactions on antennas and propagation, 2019, 67(5): 3358 – 3365. DOI: 10.1109/TAP.2019.2894260
[65] ELMOSSALLAMY M A, ZHANG H L, SONG L Y, et al. Reconfigurable intelligent surfaces for wireless communications: principles, challenges, and opportunities [J]. IEEE transactions on cognitive communications and networking, 2020, 6(3): 990 – 1002. DOI: 10.1109/TCCN.2020.2992604
[66] BASAR E, DI RENZO M, DE ROSNY J, et al. Wireless communications through reconfigurable intelligent surfaces [J]. IEEE access, 2019, 7: 116753 – 116773. DOI: 10.1109/ACCESS.2019.2935192
[67] WU Q Q, ZHANG R. Intelligent reflecting surface enhanced wireless network via joint active and passive beamforming [J]. IEEE transactions on wireless communications, 2019, 18(11): 5394 – 5409. DOI: 10.1109/TWC.2019.2936025
[68] YANG X X, JIANG C, ELSHERBENI A Z, et al. A novel compact printed rectenna for data communication systems [J]. IEEE transactions on antennas and propagation, 2013, 61(5): 2532 – 2539. DOI: 10.1109/TAP.2013.2244550
[69] LU P, YANG X S, WANG B Z. A two-channel frequency reconfigurable rectenna for microwave power transmission and data communication [J]. IEEE transactions on antennas and propagation, 2017, 65(12): 6976 – 6985. DOI: 10.1109/TAP.2017.2766450
[70] CLARKE R H, BROWN J. Diffraction theory and antennas [M]. Chichester, UK: Halsted Press, 1980. DOI: 10.1016/0029-8018(81)90030-5
[71] HAN J Q, LI L, LIU G Y, et al. A wideband 1 bit 12 × 12 reconfigurable beam-scanning reflectarray: design, fabrication, and measurement [J]. IEEE antennas and wireless propagation letters, 2019, 18(6): 1268 – 1272. DOI: 10.1109/LAWP.2019.2914399
[72] ZHANG S, XUE H, CHANG M Y, et al. Generation of airy beams using an amplitude-phase-modulated metasurface [C]//Proceedings of 2021 IEEE MTT-S International Microwave Workshop Series on Advanced Materials and Processes for RF and THz Applications. IEEE, 2021: 332 – 334. DOI: 10.1109/IMWS-AMP53428.2021.9643966
[73] ZHANG W Z, SONG C Y, PEI R, et al. Broadband metasurface antenna using hexagonal loop-shaped unit cells [J]. IEEE access, 2020, 8: 223797 – 223805. DOI: 10.1109/ACCESS.2020.3043656
[74] YU F, YANG X X, ZHONG H T, et al. Polarization-insensitive wide-angle-reception metasurface with simplified structure for harvesting electromagnetic energy [J]. Applied physics letters, 2018, 113(12): 123903. DOI: 10.1063/1.5046927
[75] XU P, WANG S Y, W G Y. Design of an effective energy receiving adapter for microwave wireless power transmission application [J]. AIP advances, 2016, 6(10): 105010. DOI: 10.1063/1.4966050
[76] ZHANG X M, LIU H X, LI L. Electromagnetic power harvester using wide-angle and polarization-insensitive metasurfaces [J]. Applied sciences, 2018, 8(4): 497. DOI: 10.3390/app8040497
[77] SONG C M, TRINH-VAN S, YI S H, et al. Analysis of received power in RF wireless power transfer system with array antennas [J]. IEEE access, 2021, 9: 76315 – 76324. DOI: 10.1109/ACCESS.2021.3083270
[78] CHEN L, MA Q, JING H B, et al. Space-energy digital-coding metasurface based on an active amplifier [J]. Physical review applied, 2019, 11(5): 054051. DOI: 10.1103/physrevapplied.11.054051
[79] MA Q, CHEN L, JING H B, et al. Controllable and programmable nonreciprocity based on detachable digital coding metasurface [J]. Advanced optical materials, 2019, 7(24): 1901285. DOI: 10.1002/adom.201901285
[80] QIU T S, JIA Y X, WANG J F, et al. Controllable reflection-enhancement metasurfaces via amplification excitation of transistor circuit [J]. IEEE transactions on antennas and propagation, 2021, 69(3): 1477 – 1482. DOI: 10.1109/TAP.2020.3019351
[81] TANG W K, DAI J Y, CHEN M Z, et al. MIMO transmission through reconfigurable intelligent surface: System design, analysis, and implementation [J]. IEEE journal on selected areas in communications, 2020, 38(11): 2683 – 2699. DOI: 10.1109/JSAC.2020.3007055
[82] HUANG C W, HU S, ALEXANDROPOULOS G C, et al. Holographic MIMO surfaces for 6G wireless networks: opportunities, challenges, and trends [J]. IEEE wireless communications, 2020, 27(5): 118 – 125. DOI: 10.1109/

MWC.001.1900534
[83] SHLEZINGER N, DICKER O, ELDAR Y C, et al. Dynamic metasurface antennas for uplink massive MIMO systems [J]. IEEE transactions on communications, 2019, 67(10): 6829–6843. DOI: 10.1109/TCOMM.2019.2927213
[84] TIAN S C, ZHANG X M, WANG X, et al. Recent advances in metamaterials for simultaneous wireless information and power transmission [J]. Nanophotonics, 2022: 1–27. DOI: 10.1515/nanoph-2021-0657
[85] WANG X, HAN J Q, TIAN S C, et al. Amplification and manipulation of nonlinear electromagnetic waves and enhanced nonreciprocity using transmissive space-time-coding metasurface [J]. Advanced science, 2022, 9(11): 2105960. DOI: 10.1002/advs.202105960
[86] ZHANG P, ZHANG X M, LI L. An optically transparent metantenna for RF wireless energy harvesting [J]. IEEE transactions on antennas and propagation, 2022, 70(4): 2550–2560. DOI: 10.1109/TAP.2021.3137166
[87] LI L, ZHANG P, HAN J, et al. Key technologies of microwave wireless power transfer and energy harvesting based on electromagnetic metamaterials [J]. Acta photonica sinica, 2021, 50(10): 1016001. DOI: 10.3788/gzxb20215010.1016001

Biographies

CHANG Mingyang received the BE degree in electronic information science and technology from Yantai University, China in 2018. He is currently pursuing the PhD degree in electromagnetic fields and microwave technology at Xidian University, China. His research interests include wireless power transfer, wireless energy harvesting, metasurfaces, and simultaneous wireless information and power transfer.

HAN Jiaqi received the BE degree in electronic and information engineering from Henan Normal University, China in 2014, and the PhD degree in electromagnetic fields and microwave technology from Xidian University, China in 2019. He is currently a post-doctoral fellow with the School of Electronic Engineering, Xidian University. His research interests include the design of programmable metasurfaces and their applications on wireless power transfer and computational imaging.

MA Xiangjin received the BE degree in communication engineering from Nanchang Institute of Technology, China in 2019. He is currently pursuing the PhD degree in electromagnetic field and microwave technology at Xidian University, China. His current research interests include analysis and application of programmable metasurfaces, design of high-performance programmable metasurfaces and microwave holographic imaging.

XUE Hao received the BE degree in electronic and information engineering from Xidian University, China in 2015. He is currently pursuing the PhD degree in electronic science and technology at Xidian University. His research interests include antenna design, metasurface, wireless power transfer, and OAM vortex beam. He received the honors and awards include the National scholarship for postgraduates 2017, the Best Student Paper Awards of IEEE iWAT 2018, and IEEE IMWS-AMP 2021.

WU Xiaonan received the BE degree in electronic information engineering from Xidian University, China in 2020. He is currently pursuing the master's degree in electromagnetic field and microwave technology at Xidian University. His research interests include wireless power transfer, wireless energy harvesting, design of metasurfaces, and simultaneous wireless information and power transfer.

LI Long (lilong@mail.xidian.edu.cn) received the BE and PhD degrees in electromagnetic fields and microwave technology from Xidian University, China in 1998 and 2005, respectively. He is currently a professor in the School of Electronic Engineering, Xidian University. Prof. LI is the Director of Key Laboratory of High-Speed Circuit Design and EMC, Ministry of Education, China. His research interests include metamaterials/metasurfaces, antennas and microwave devices, wireless power transfer and harvesting technology, and OAM vortex waves. He has published over 180 papers in journals and held more than 40 patents. Prof. LI was awarded the Chang Jiang Scholars Distinguished Professor by Ministry of Education, China in 2021. Prof. LI is the Vice-President of MTT-Chapter in IEEE Xi'an Section. He is a TPC Co-Chair of APCAP2017 and a General Co-Chair of AWPT2019.

CUI Tiejun (tjcui@seu.edu.cn) received the BS, MS, and PhD degrees in electrical engineering from Xidian University, China in 1987, 1990, and 1993, respectively. He is currently the Chief Professor of Southeast University, China. Prof. CUI is the Academician of Chinese Academy of Science and an IEEE Fellow. Prof. CUI's research interests include metamaterials and computational electromagnetics. He proposed the concepts of digital coding and programmable metamaterials, and realized their first prototypes, based on which he founded the new direction of information metamaterials, bridging the physical world and digital world. He has published over 500 peer-review journal papers, which have been cited by more than 43 000 times (H-Factor 105, Google Scholar), and licensed over 150 patents. Prof. CUI was awarded a Cheung Kong Professor by the Ministry of Education, China in 2001, and received the National Science Foundation of China for Distinguished Young Scholars in 2002. Prof. CUI received the Natural Science Award (first class) from the Ministry of Education, China in 2011, and the National Natural Science Awards of China (second class, twice) in 2014 and 2018, respectively.